Electronic Supplementary Material (ESI) for Nanoscale Advances.

Supporting Information For:

Assessing the Bio-stability of microRNA-146a conjugated Nanoparticles via Electroanalysis

Chaimae El Ghzaoui, [a] Craig J. Neal, [a] Elayaraja Kolanthai, [a] Yifei Fu, [a] Udit Kumar, [a] Junyi Hu, [b] Carlos Zgheib, [b] Kenneth W. Liechty [b] and Sudipta Seal * [a,c]

[a] *Advanced Materials Processing and Analysis Center, Dept. of Materials Science and Engineering, University of Central Florido, Orlando, FL, USA*

[b] *Laboratory for Fetal and Regenerative Biology, Department of Surgery, University of Arizona School of Medicine and Diamond Children's Hospital, Tucson, Arizona, USA*

[c] *College of Medicine, Nanoscience Technology Center, Biionix Cluster, University of Central Florida, Orlando, FL, USA*

Email: Sudipta.seal@ucf.edu

Estimate of the theoretical number of miR146a per nanoparticle

The theoretical calculations to measure the ratio have been performed based on the assumption of the spherical shape of the particles and using the theoretical density of AuNP (19.3 g/cm^3), SiO_2NP (2.65 g/cm^3), and CNP (7.22 g/cm^3).

For calculating the number of nanoparticles, we have used this equation:

$$N_p = \frac{Total\ mass\ of\ the\ nanoparticles\ sample}{mass\ of\ one\ nanoparticle} = \frac{m}{\rho * \frac{4}{3}\pi * r^3}$$

Where N_p is the number of nanoparticles, m is the total mass of the nanoparticles, ρ is the theoretical density, and r is the radius of nanoparticle obtained from TEM.

The number of miR146a is calculated according to the following equation:

$$N_{miR} = C*V*N_A*1/M$$

Where C is the mass concentration of miR146a obtained from the assay kit, V is the volume of the sample, N_A is the Avogadro number, and M is the molar mass of miR146a.

The ratio of the number of miR146a per nanoparticle is: $\frac{N_{miR}}{N_p}$

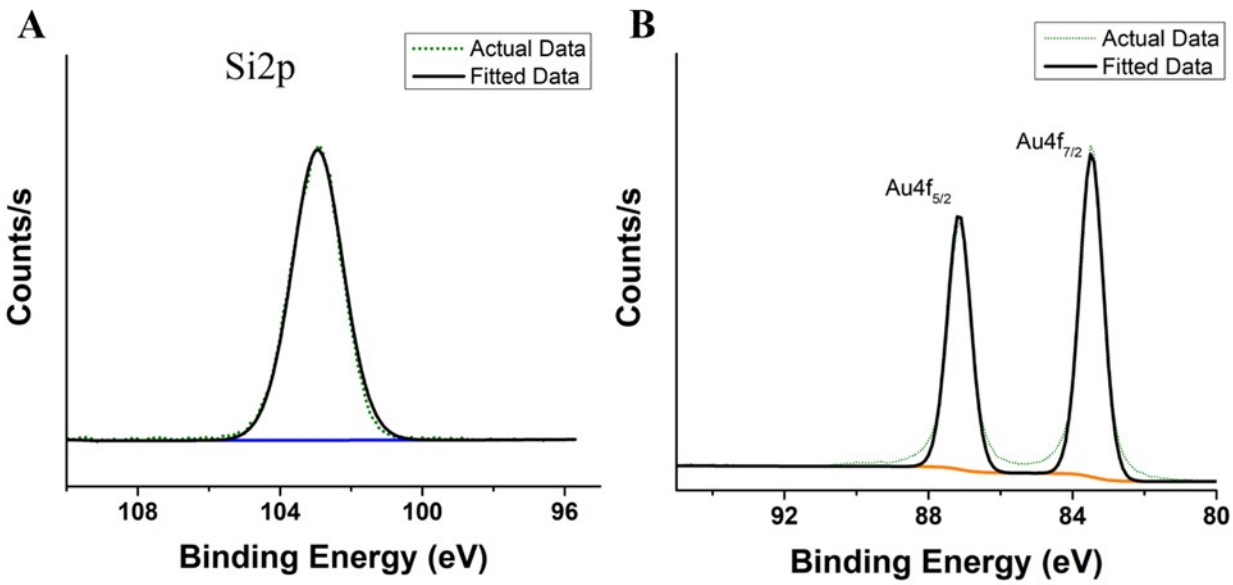

Figure S1. XPS characterization of nano formulations. XPS scans for control SiO2NP and AuNP are shown in (a) Si2p, and (b) Au4f, respectively. Si2p scan shows a broad peak corresponding to Si-O interactions. Au4f scan shows a doublet peak corresponding to elemental Au.

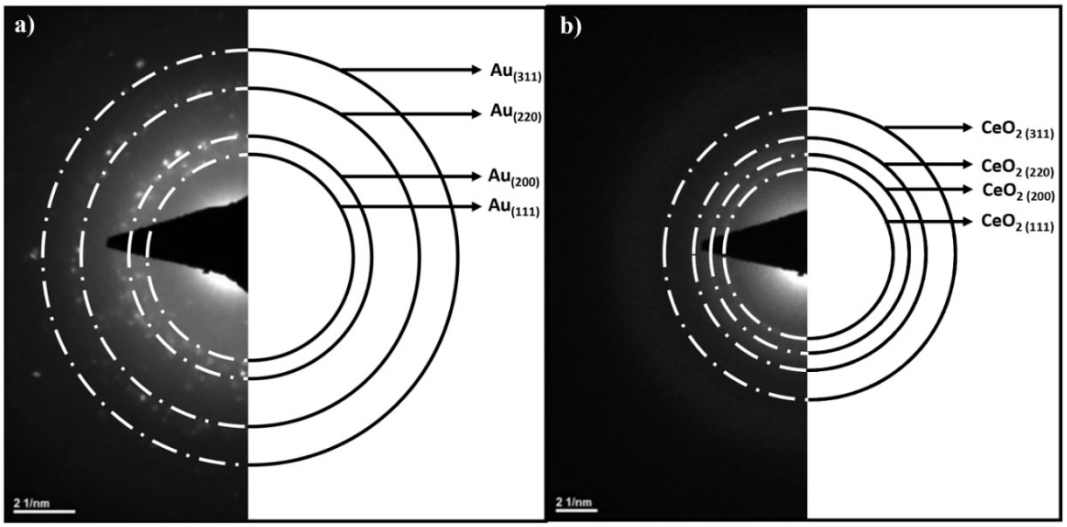

Figure S2. Selected area electron diffraction (SAED) pattern. Both (a) AuNP-miR146a and (b) CNP-miR146a SAED patterns confirm particle crystallinity. Crystal planes of fluorite crystal structure from cerium oxide and face center cubic crystal structure from gold are determined and noted in the image.

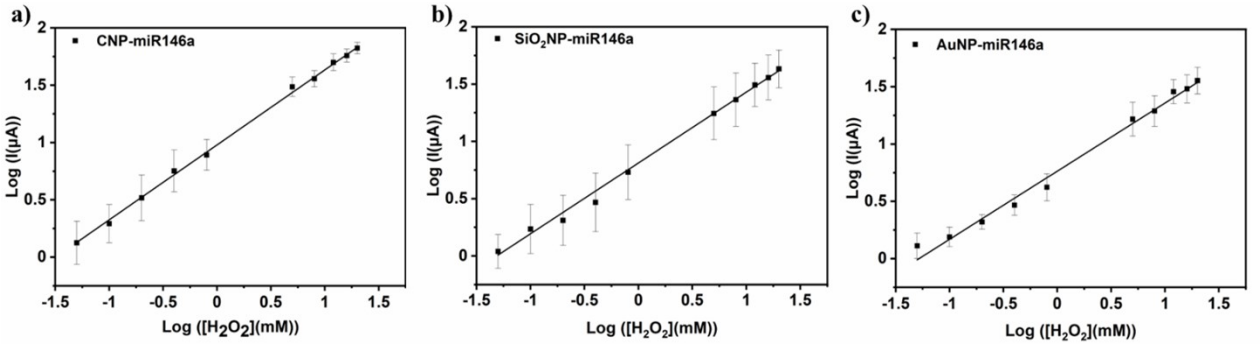

Figure S3. Calibration curves plots after chronoamperometry measurements. Calibration curves plots of log I vs. log [H_2O_2] in the range between log (0.05 mM) to log (20 mM) for (a) CNP-miR146a, (b) SiO_2NP-miR146a, and (c) AuNP-miR146a

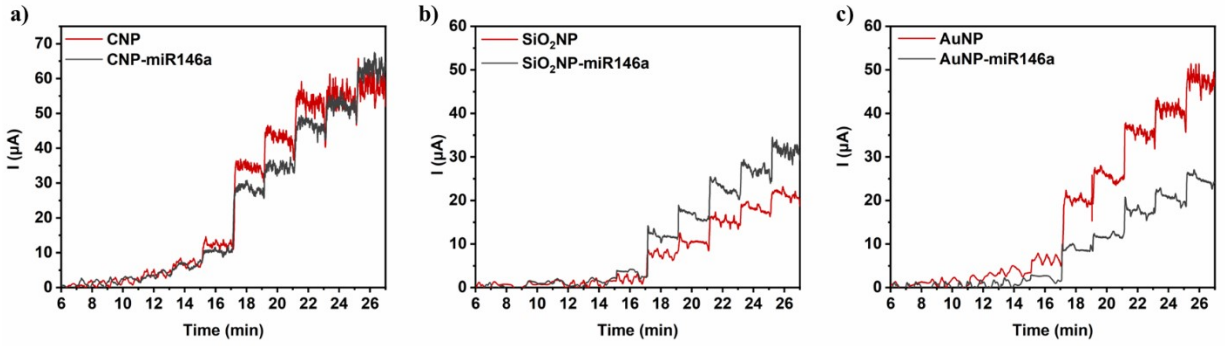

Figure S4. Chronoamperometry measurements (CA). CA conducted on modified glassy carbon electrode by (a) CNP, CNP-miR146a, (b) SiO_2NP, SiO_2NP-miR146a, and (c) AuNP, AuNP-miR146a emerged in 10 mM PBS with successive addition of H_2O_2, achieving total H_2O_2 concentrations in the electrolyte solution of 0.05, 0.1, 0.2, 0.4, 0.8, 5, 8, 12, 16, 20 mM with an interval time of 2 min between each addition. The first H_2O_2 addition was conducted after 7 min of CA measurement in 10 mM PBS.

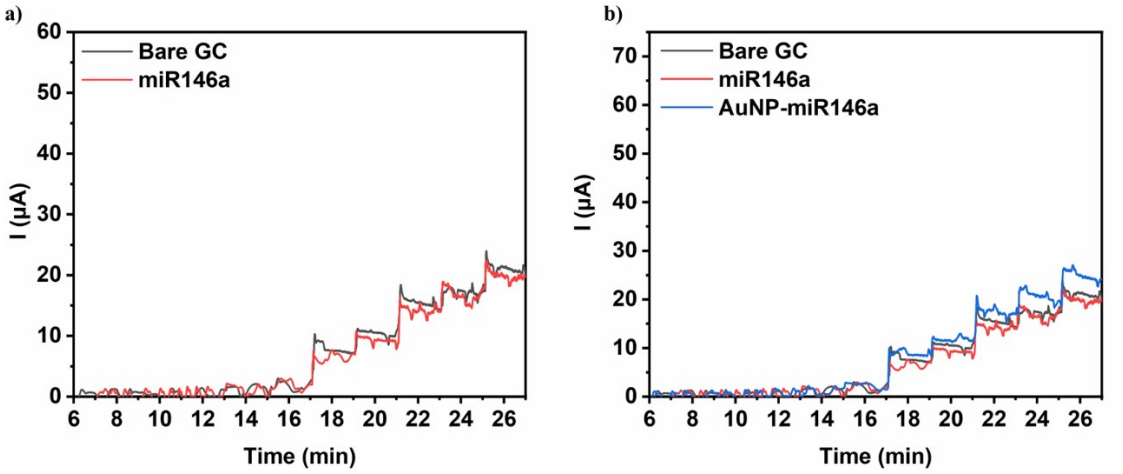

Figure S5. Chronoamperometry measurements (CA). CA conducted on (a) non-modified glassy carbon electrode, and modified glassy carbon electrode by bare miR46a, (b) modified glassy carbon electrode by AuNP-miR146a, bare miR46a, and non-modified glassy carbon electrode emerged in 10 mM PBS with successive addition of H_2O_2, achieving total H_2O_2 concentrations in the electrolyte solution of 0.05, 0.1, 0.2, 0.4, 0.8, 5, 8, 12, 16, 20 mM with an interval time of 2 min between each addition. The first H_2O_2 addition was conducted after 7 min of CA measurement in 10 mM PBS.

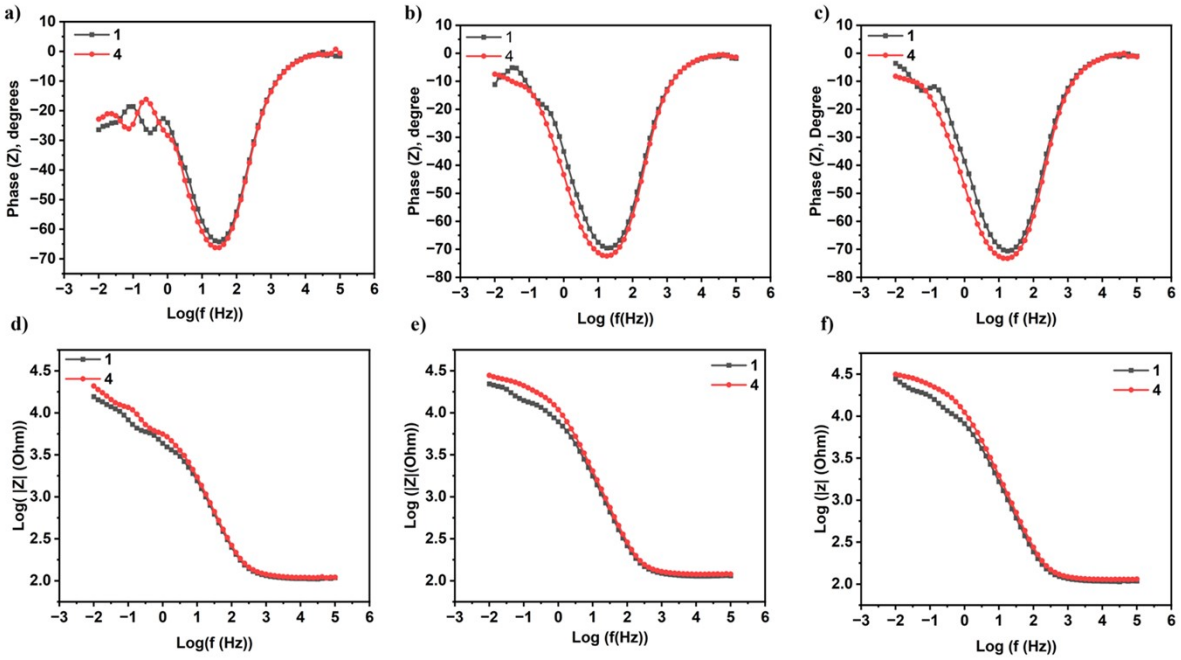

Figure S6. Impedance data in Bode representation of modified glassy carbon (GC) electrode in PBS/H_2O_2 (10 mM/10 mM) solution at 0.65V (potential of instability for H_2O_2). Four continuous successive repeats of the EIS measurements were conducted in the same electrolyte for each sample, and the first (1) and the fourth (4) spectra were represented in the bode diagram. The bode plots of the phase angle vs. frequency of (a) CNP-miR146a, (b) AuNP-miR146a, and (c) SiO_2NP-miR146a and the bode plots of impedance magnitude vs. frequency of (d) CNP-miR146a, (e) AuNP-miR146a, and (f) SiO_2NP-miR146a show the changes of the modified GC electrode surface with each sample due to the exposure of unstable H_2O_2.

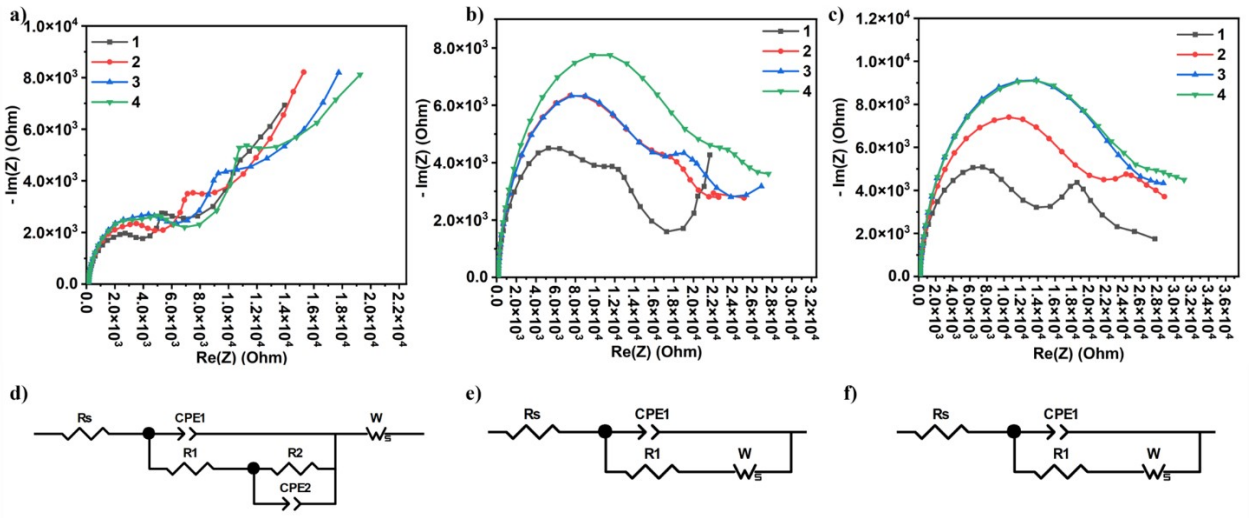

Figure S7. Electrochemical impedance spectroscopy. Nyquist plots of modified glassy carbon (GC) electrode in PBS/H_2O_2 (10 mM/10 mM) solution at 0.65V (potential of instability for H_2O_2) with four continuous, successive repeats (plotted as 1 - 4) of the EIS measurements in the same electrolyte for each of (a) CNP-miR146a, (b) AuNP-miR146a, and (c) SiO_2NP-miR146a. The spectra of the fourth repeat were fitted by ZView software, and the equivalent circuits for (d) CNP-miR146a, (e) AuNP-miR146a, and (f) SiO_2NP-miR146a are presented. R_s is the solution resistance, R_1/R_2 is the charge transfer resistances, W is the Warburg diffusion element, and CPE_1/CPE_2 is the constant phase element of the non-ideal capacitance of the double layer. (can u say what are 1, 2, 3, 4

Table S1. FTIR analysis of the effect of 6 hours exposed to SiO_2NP-miR146a, AuNP-miR146a, and SiO_2NP-miR146a to 10mM H_2O_2. The consequential alterations in peaks centers and the area of the peaks with band frequency assignment are summarized in this table.

SiO_2NP-miR146a before H_2O_2		**SiO_2NP-miR146a after H_2O_2**		**Changes**		
Peak Center	**Peak Area**	**Peak Center**	**Peak Area**	**Shifted by (Cm^{-1})**	**% Area Change**	**Peak Assignment (Reference 1-8)**
951	442.3	950	335	-1	-24.3	C-O, C-C
1021	979.7	1018.5	496.6	-2.5	-49.3	C-O stretch, Si-O-Si
1103.5	1515.1	1099	1311.2	-4.5	-13.5	PO^{2-} symmetric
1353.5	153.5	1353.5	191.9	0	25.1	(C-N, C=O) amide stretch
1413.5	370.3	1413.5	722.5	0	95.1	C-H, C-N, N-H
1648.5	2160.5	1647	2284.9	-1.5	5.8	(N-H, C=O, C=C) stretch, Si-H_2O
2919.5	885.1	2925	261.2	5.5	-70.5	Stretch C-H, SiO-H
3427.5	8773	3426	8401.3	-1.5	-4.2	N-H, OH stretch

AuNP-miR146a before H_2O_2		**AuNP-miR146a after H_2O_2**		**Changes**		
Peak Center	**Peak Area**	**Peak Center**	**Peak Area**	**Shifted by (Cm^{-1})**	**% Area Change**	**Peak Assignment (Reference 1, 2, 4-6)**
952	479.7	951.5	370.2	-0.5	-22.8	C-O, C-C
1019	1474.8	1018.5	1032	-0.5	-30	C-O stretch
-------	-------	1096	350	-------	-------	PO^{2-} symmetric
1317.5	171.7	1321	277.6	3.5	61.7	(C-N, C=O) amide stretch
1432	426.6	1433	692.3	1	62.3	C-H, C-N, N-H
1653.5	2557.7	1650.5	2405	-3	-6	(N-H, C=O, C=C) stretch
2922	548.6	2927	538	5	-1.9	Stretch C-H
3461.5	7656.3	3451	8458.4	-10.5	10.5	N-H, OH stretch

CNP-miR146a before H_2O_2		**CNP-miR146a after H_2O_2**		**Changes**		
Peak Center	**Peak Area**	**Peak Center**	**Peak Area**	**Shifted by (Cm^{-1})**	**% Area Change**	**Peak Assignment (Reference 1, 2, 4-6)**
951.5	499	951	316. 3	-0.5	-36.6	C-O, C-C
1018.5	1155.7	1017.5	824.8	-1	-28.6	C-O stretch
1092.5	313.5	1095.5	419.5	3	33.8	PO^{2-} symmetric
1351.5	450.3	1346.5	905.2	-5	101	(C-N, C=O) amide stretch
1413	1603.5	1414	1454.7	1	-9.3	C-H, C-N, N-H
1654.5	2411.4	1647.5	2917.3	-7	21	(N-H, C=O, C=C) stretch
3447	6834	3447	10752.7	0	57.3	N-H, OH stretch

Table S2. From C1s binding region XPS measurements, the ratio of the peak area at 288 eV corresponding to O-C=C to the sum of all C1s peaks of each formulation incubated with 10 and 500 mM hydrogen peroxide for 6 hours was calculated and presented in this table.

Samples	**Peak Area ratio** $A_{O\text{-}C=C} / \Sigma A_{C1s}$
CNP-miR146a 10 mM H_2O_2	0.072011
CNP-miR146a 500 mM H_2O_2	0.061145
AuNP-miR146a 10 mM H_2O_2	0.056328
AuNP-miR146a 500 mM H_2O_2	0.115744
SiO_2-NP-miR146a 10 mM H_2O_2	0.285931
SiO_2-NP-miR146a 500 mM H_2O_2	0.411976

References

1. Dewberry LC, Niemiec SM, Hilton SA, Louiselle AE, Singh S, Sakthivel TS, et al. Cerium oxide nanoparticle conjugation to microRNA-146a mechanism of correction for impaired diabetic wound healing. Nanomedicine: Nanotechnology, Biology and Medicine. 2022;40:102483.
2. Dovbeshko GI, Gridina NY, Kruglova EB, Pashchuk OP. FTIR spectroscopy studies of nucleic acid damage. Talanta. 2000;53(1):233-46.
3. Żeglin J, Piotrowski GP, Piękos R. A study of interaction between hydrogen peroxide and silica gel by FTIR spectroscopy and quantum chemistry. Journal of molecular structure. 2006;794(1-3):83-91.
4. Tajmir-Riahi H, N'Soukpoe-Kossi C, Joly D. Structural analysis of protein–DNA and protein–RNA interactions by FTIR, UV-visible and CD spectroscopic methods. Spectroscopy. 2009;23(2):81-101.
5. Prakash C, Kamboj VK, Ahlawat P, Kumar V. Structural and molecular alterations in arsenic-induced hepatic oxidative stress in rats: a FTIR study. Toxicological & Environmental Chemistry. 2015;97(10):1408-21.
6. Gault N, Rigaud O, Poncy J-L, Lefaix J-L. Infrared microspectroscopy study of γ-irradiated and H2O2-treated human cells. International journal of radiation biology. 2005;81(10):767-79.
7. Dubey R, Rajesh Y, More M. Synthesis and characterization of SiO2 nanoparticles via sol-gel method for industrial applications. Materials Today: Proceedings. 2015;2(4-5):3575-9.
8. El Rassy H, Pierre A. NMR and IR spectroscopy of silica aerogels with different hydrophobic characteristics. Journal of Non-Crystalline Solids. 2005;351(19-20):1603-10.